Fuselage Boundary-Layer Effects on Sound Propagation and Scattering

H. Y. Lu*
Boeing Commercial Airplanes, Seattle, Washington 98124

The effects of a fuselage and its boundary layer on sound propagation to the fuselage surface and on sound scattering in the farfield were analyzed. A hard-wall infinite cylinder with a boundary layer of both velocity and temperature variations was modeled to simulate the fuselage of an aircraft in flight. Examples for a monopole noise source outside the boundary layer showed considerable noise attenuation on the cylindrical surface forward of the source and much less effect on the downstream side. Data from a transonic wind tunnel test showed the same trends. For enroute and airport community noise, the boundary layer alters the interference pattern caused by the fuselage.

Nomenclature

c = dimensionless speed of sound (normalized by c_0)
c_0 = reference speed, speed of sound in the uniform mean flow (freestream) region
f = frequency
k_x = dimensionless wave number (normalized by $1/R_f$)
L = boundary-layer thickness
M = freestream Mach number
n = angular mode number, integer
p = dimensionless acoustic pressure (normalized by $\rho_0 c_0^2$)
Q = dimensionless source distribution (normalized by $\rho_0 c_0/R_f$)
r = R/R_f
r_b = dimensionless radius of the boundary-layer edge (normalized by R_f)
R = radial coordinate, defined specifically if used otherwise
R_f = reference length, fuselage radius
t = dimensionless time (normalized by R_f/c_0)
T_0 = absolute temperature in the freestream
T_f = absolute temperature at the fuselage surface
U = dimensionless axial mean flow velocity in boundary layer (normalized by c_0)
x = X/R_f
X = axial coordinate, downstream direction positive
θ = angle in cylindrical coordinates, right-hand system
ω = dimensionless angular frequency (normalized by c_0/R_f)
ρ_0 = reference density, freestream density
λ_0 = c_0/f

Introduction

ADVANCED propeller engines have been proposed for use on future commercial aircraft. In support of airplane design studies, assessment is needed for the impact of propeller noise on cabin interior noise, sonic fatigue, airport community, and enroute noise. However, current propeller noise prediction methods have been developed to predict freefield noise levels without including the influence of the fuselage and its boundary layer. The change in sound pressure level (SPL) from the freefield to that with the presence of a fuselage and its boundary layer can be several dB in the farfield and much greater on the fuselage surface. Predictions of "installed" propeller noise level on the fuselage and in the farfield need to include the effects of the fuselage and its boundary layer.

Previous work in this area includes that of Hanson and Magliozzi.[1] They modeled the fuselage and boundary-layer effects by using an infinite cylinder with an isothermal thin boundary layer. A rotating source in uniform flow is used to simulate the propeller noise. A substantial reduction in SPL from freefield plus 6 dB (i.e., pressure doubling) was predicted in the forward direction on the fuselage surface at high subsonic Mach numbers. McAninch and Rawls, Jr.[2] and McAninch[3] analyzed a flat plate model with boundary layer and plane incident waves. The effect of a wake inside the boundary layer was calculated.[3]

The present analytical model is similar to that of Hanson and Magliozzi; however, without the simplification of the thin and isothermal boundary-layer assumptions. The analysis covers both the nearfield case for application to a fuselage surface and the farfield case for flyover noise application. A boundary layer of arbitrary constant thickness with velocity and temperature variations in the radial direction is used in the analysis. For a fuselage-mounted pusher propeller, the boundary layer is not considered "thin" relative to the local radius of the fuselage.

The analysis assumes that the acoustic freefield is given. The acoustic field, due to the presence of the fuselage cylinder and its boundary layer, is calculated for the given freefield. The difference in SPL at a point on the fuselage with the boundary layer and the SPL of the uniform flow freefield at the same point is calculated. This difference includes the source directivity difference caused by boundary-layer refraction. If the source has a very smooth directivity, then the SPL difference due to the directivity change will be small. A monopole in a subsonic flow provides a smoother directivity than other types of sources, and is used as an example for calculating the SPL differences for parametric comparisons.

Of equal importance is evaluation of this installation effect in the farfield, as well as that for the nearfield on the fuselage surface. An asymptotic solution is provided for calculating the installation effect on community noise and on enroute noise levels.

A counter-rotating model propeller was tested in a transonic wind tunnel and provided data on boundary-layer effects. The test data are compared with predictions, using a monopole noise source, and the results are discussed.

Received Feb. 17, 1989; presented as Paper 89-1098 at the AIAA 12th Aeroacoustics Conference, San Antonio, TX, April 10-12, 1989; revision received May 15, 1989.

*Senior Engineer.

Analysis

A schematic of the basic model is shown in Fig. 1. The fuselage is represented by an infinite and rigid cylinder of radius R_f. The boundary layer is assumed to have a uniform thickness L over the cylindrical surface. Outside the boundary layer, the basic flow is constant in velocity and temperature (or speed of sound). The cylindrical coordinates R, θ, and X form a right-handed system, as shown with the X-axis coincident with the fuselage axis and positive in the direction from nose to tail. All the parameters are made dimensionless in the analysis with the reference parameters defined in the Nomenclature.

Sound Propagation in Parallel Shear Flow

The linearized equation for pressure disturbances in parallel shear flow is derived from basic equations of flow and thermodynamics, as shown by Goldstein.[4] The homogeneous equation (without a source) term is

$$\frac{D_0}{Dt}\left(\nabla^2 p + 2\frac{c'}{c}\frac{\partial p}{\partial r} - \frac{1}{c^2}\frac{D_0^2 p}{Dt^2}\right) - 2U'\frac{\partial^2 p}{\partial x \partial r} = 0 \tag{1}$$

where

$$\frac{D_0}{Dt} = \frac{\partial}{\partial t} + U\frac{\partial}{\partial x}$$

$$\nabla^2 = \frac{1}{r}\frac{\partial}{\partial r}\left(r\frac{\partial}{\partial r}\right) + \frac{1}{r^2}\frac{\partial^2}{\partial \theta^2} + \frac{\partial^2}{\partial x^2}$$

$$c' = \mathrm{d}c/\mathrm{d}r$$

$$U' = \mathrm{d}U/\mathrm{d}r$$

Fourier transform of Eq. (1) yields

$$(\omega - Uk_x)\frac{\mathrm{d}^2 F}{\mathrm{d}r^2} + \left[(\omega - Uk_x)\left(\frac{1}{r} + 2\frac{c'}{c}\right) + 2U'k_x\right]\frac{\mathrm{d}F}{\mathrm{d}r} + (\omega - Uk_x)\left[\frac{(\omega - Uk_x)^2}{c^2} - \left(k_x^2 + \frac{n^2}{r^2}\right)\right]F = 0 \tag{2}$$

where

$$F = \frac{1}{8\pi^3}\int_{-\infty}^{\infty}\int_{-\infty}^{\infty}\int_0^{2\pi} p e^{i(\omega t - k_x x - n\theta)}\,\mathrm{d}\theta\,\mathrm{d}x\,\mathrm{d}t$$

The complex acoustic pressure for a given angular frequency ω is represented by the following integral:

$$p_\omega = \sum_{n=-\infty}^{\infty} e^{in\theta} F \int_{-\infty}^{\infty} (r; n, k_x, \omega) e^{ik_x x}\,\mathrm{d}k_x \tag{3}$$

Inside the Boundary Layer

The boundary extends from $r = 1$ on the fuselage surface to $r = r_b$ at the edge of the boundary layer. A numerical integration method is used to find $F(r)$ by letting $F(1) = 1$ as the unit magnitude and $F'(1) = 0$ for hard wall boundary condition in parallel mean flow. $F(1)$ will be multiplied by a complex coefficient to be determined later by matching the solution at the edge of the boundary layer. However, at $r = r_c$ where

$$\omega - U(r_c)k_x = 0$$

the equation is singular. This occurs since Eq. (3) is an integration over all the real k_x values, including those for the nearfield pressure. In the asymptotic solution for the farfield to be provided later, this singularity will not occur for the subsonic flow.

The Frobenius series solution[5] is used as a bridge to allow the numerical integration to continue on the other side of the singularity up to $r = r_b$. The Frobenius series solution is provided in the Appendix.

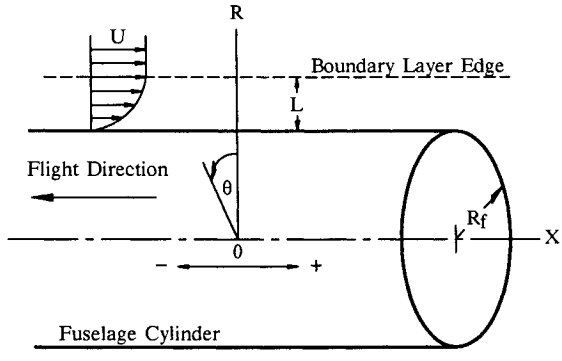

Fig. 1 Schematic model of a fuselage cylinder with a boundary layer.

Outside the Boundary Layer

A uniform mean flow, $U = M$, $U' = 0$, $c = 1$, and $c' = 0$, is assumed. Equation (2) is reduced to

$$\frac{\mathrm{d}}{\mathrm{d}r}\left(r\frac{\mathrm{d}F}{\mathrm{d}r}\right) + \left(\zeta^2 r - \frac{n^2}{r}\right)F = 0 \tag{4}$$

where

$$\zeta^2 = (\omega - Mk_x)^2 - k_x^2 \tag{5}$$

and the solution takes the form

$$F = a_n J_n(\zeta r) + b_n H_n^{(1)}(\zeta r) \tag{6}$$

where J_n and $H_n^{(1)}$ are the Bessel function and the Hankel function of order n, respectively.

For acoustic sources outside the boundary layer the incident acoustic field; i.e., the freefield without the fuselage and its boundary layer is represented by $a_n J_n(\zeta r)$, since the freefield acoustic pressure is not unbounded at $r = 0$ on the fuselage axis. The scattered acoustic field outside the fuselage boundary layer takes the form $b_n H_n^{(1)}(\zeta r)$ for the unbounded space to satisfy the radiation condition. It is assumed that the incident field is given; i.e., the coefficient a_n is known. The coefficient b_n will be determined by matching the solution at the edge of the boundary layer.

Matching the Solution at the Edge of the Boundary Layer

The solution inside the boundary layer was obtained numerically by letting $F(1) = 1$ on the fuselage surface. This solution multiplied by a constant is matched with the solution outside the boundary layer at the edge of the boundary layer. Since the flow properties are continuous across the edge of the boundary layer, the pressure and its derivative are also continuous, i.e.,

$$\alpha_n F(r_b) = a_n J_n(\zeta r_b) + b_n H_n^{(1)}(\zeta r_b)$$

$$\alpha_n F'(r_b) = a_n \zeta J_n'(\zeta r_b) + b_n \zeta H_n^{(1)'}(\zeta r_b)$$

These two conditions are solved to provide

$$\alpha_n = 2ia_n/(\pi r_b E) \tag{7}$$

$$b_n = a_n\left[J_n(\zeta r_b)F'(r_b) - \zeta J_n'(\zeta r_b)H_n^{(1)}(\zeta r_b)\right]/E \tag{8}$$

where

$$E = F(r_b)\zeta H_n^{(1)'}(\zeta r_b) - F'(r_b)H_n^{(1)}(\zeta r_b) \tag{9}$$

is the determinant of coefficients in matching.

Effects on Fuselage Surface SPL

For an angular frequency ω, the complex acoustic pressure on the fuselage surface is given by

$$p_\omega(1) = \sum_{n=-\infty}^{\infty} e^{in\theta} \int_{-\infty}^{\infty} \alpha_n e^{ik_x x}\, dk_x \tag{10}$$

since $F(1) = 1$ was used as a starting point for numerical integration.

The incident freefield complex acoustic pressure at the same point is

$$p_{i\omega}(1) = \sum_{n=-\infty}^{\infty} e^{in\theta} \int_{-\infty}^{\infty} a_n J_n(\zeta) e^{ik_x x}\, dk_x \tag{11}$$

where $a_n(k_x,\omega)$ is assumed to be given.

The increase in SPL at the fuselage surface, $\mathrm{SPL}_{\mathrm{fuselage}}$, from that of the freefield level, $\mathrm{SPL}_{\mathrm{freefield}}$, at the same location is

$$\mathrm{SPL}_{\mathrm{fuselage}} - \mathrm{SPL}_{\mathrm{freefield}} = 20 \log\left[\, |p_\omega(1)/p_{i\omega}(1)| \,\right] \tag{12}$$

which can be compared with 6 dB for the case of a rigid infinite flat plate without a boundary layer.

Effects on Farfield SPL

For a confined source region with the maximum extension at $r = r_{\max}$, the outgoing waves from the source is $D_n H_n^{(1)}(\zeta r)$, where D_n is the known coefficient. The total farfield, including that of the scattered field for $r > r_{\max}$, is

$$F = (b_n + D_n) H_n^{(1)}(\zeta r) \tag{13}$$

where b_n has been determined.

For an angular frequency ω, the complex acoustic pressure is

$$p_\omega(r) = \sum_{n=-\infty}^{\infty} e^{in\theta} \int_{-\infty}^{\infty} (b_n + D_n) H_n^{(1)}(\zeta r) e^{ik_x x}\, dk_x \tag{14}$$

The method of stationary phase[5] is used to obtain a farfield asymptotic solution, i.e.,

$$p_\omega(r) \sim \frac{-2i}{R} \frac{e^{ihR}}{(1-M^2\sin^2\phi)^{1/2}} \sum_{n=-\infty}^{\infty} (b_n + D_n) e^{in(\theta - \pi/2)} \tag{14a}$$

where

$$R = (x^2 + r^2)^{1/2}$$

$$\phi = \cos^{-1}(x/R)$$

$$h = \zeta \sin\phi + k_x \cos\phi$$

$$\sim \frac{\omega}{1-M^2}\left[(1-M^2\sin^2\phi)^{1/2} - M\cos\phi\right]$$

$$k_x \sim k_{xs} = \frac{\omega}{1-M^2}\left[\frac{\cos\phi}{(1-M^2\sin^2\phi)^{1/2}} - M\right]$$

All the coefficients are evaluated at the stationary phase value of $k_x = k_{xs}$ given above.

Similarly the far freefield solution can be written as

$$p_{i\omega}(r) = \sum_{n=-\infty}^{\infty} e^{in\theta} \int_{-\infty}^{\infty} D_n H_n^{(1)}(\zeta r) e^{ik_x x}\, dk_x \tag{15}$$

and its stationary phase asymptotic expression is

$$p_{i\omega}(r) \sim \frac{-2i}{R} \frac{e^{ihR}}{(1-M^2\sin^2\phi)^{1/2}} \sum_{n=-\infty}^{\infty} D_n e^{in(\theta - \pi/2)} \tag{15a}$$

The increase in the farfield SPL, $\mathrm{SPL}_{\mathrm{installed}}$, for the engine installed on the fuselage from the far freefield SPL, $\mathrm{SPL}_{\mathrm{freefield}}$, of the engine alone at the same farfield location is given by

$$\mathrm{SPL}_{\mathrm{installed}} - \mathrm{SPL}_{\mathrm{freefield}} = 20 \log\left[\, |p_\omega(r)/p_{i\omega}(r)| \,\right] \tag{16}$$

with the use of the asymptotic expressions in Eqs. (14a) and (15a).

Monopole Outside the Boundary Layer

The equation for the acoustic pressure can be derived[4] by including a source distribution $Q(r,\theta,x,t)$. In the case of a monopole at $r = r_0$, $\theta = \theta_0$, and $x = x_0$, Q takes the form

$$Q = q(t)\delta(r - r_0)[\delta(\theta - \theta_0)/r]\delta(x - x_0) \tag{17}$$

The equation for F outside the boundary layer becomes

$$\frac{d}{dr}\left(r\frac{dF}{dr}\right) + \left(\zeta^2 r - \frac{n^2}{r}\right)F = \frac{i(\omega - Mk_x)}{4\pi^2} q_\omega e^{-i(k_x x_0 + n\theta_0)} \delta(r - r_0) \tag{18}$$

where

$$q_\omega = \frac{1}{2\pi}\int_{-\infty}^{\infty} q(t) e^{i\omega t}\, dt \tag{19}$$

The solution is

$$F = a_n J_n(\zeta r) + b_n H_n^{(1)}(\zeta r), \qquad r_b \le r < r_0 \tag{20}$$

and

$$F = (b_n + D_n) H_n^{(1)}(\zeta r), \qquad r > r_0 \tag{21}$$

where

$$a_n = \frac{1}{8\pi}(\omega - Mk_x) H_n^{(1)}(\zeta r_0) e^{-i(k_x x_0 + n\theta_0)} q_\omega \tag{22}$$

$$D_n = \frac{1}{8\pi}(\omega - Mk_x) J_n(\zeta r_0) e^{-i(k_x x_0 + n\theta_0)} q_\omega \tag{23}$$

are the coefficients for the incident and the outgoing freefields, respectively. They are determined by solving the freefield problem, which has continuous pressure or F, at $r = r_0$ and a jump of the pressure gradient or dF/dr, obtained by integrating Eq. (18) across $r = r_0$.

The expression of a_n is used to obtain α_n and b_n from Eqs. (7) and (8), respectively, and the effects on the fuselage surface SPL and on farfield SPL can be calculated from Eqs. (12) and (16), respectively. However, taking advantage of the axisym-

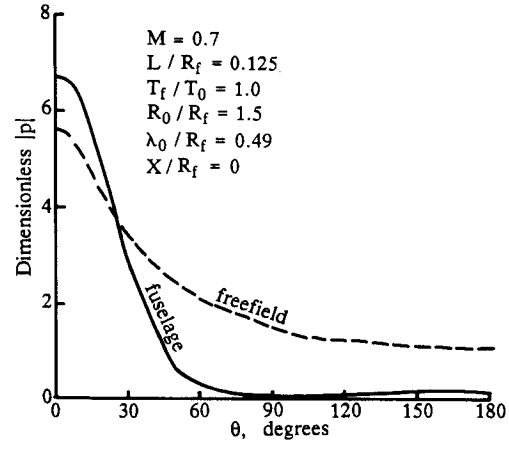

Fig. 2 Amplitude of dimensionless acoustic pressure, circumferential distribution.

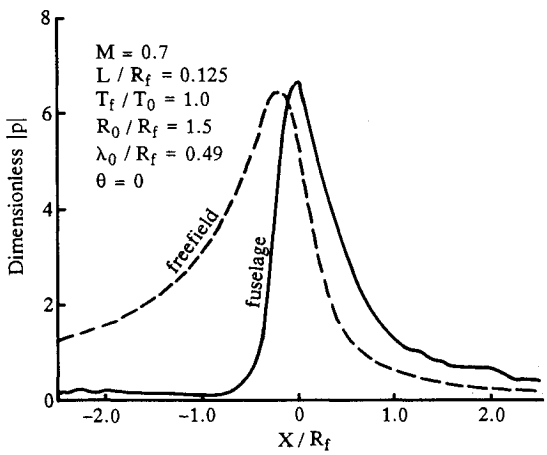

Fig. 3 Amplitude of dimensionless acoustic pressure, longitudinal distribution.

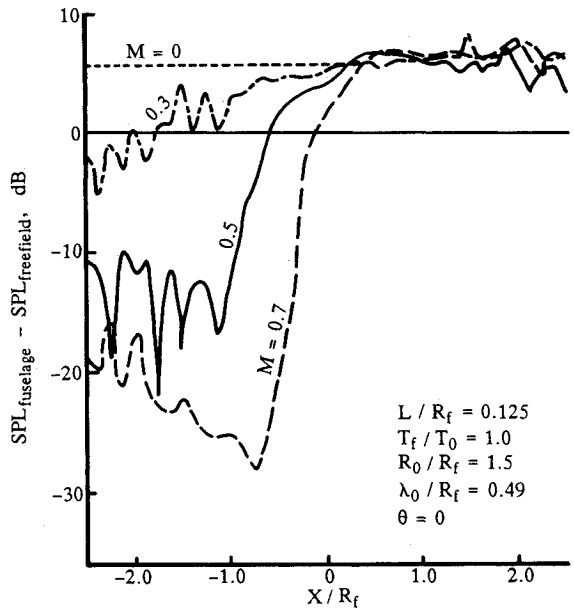

Fig. 4 Variation of effects along the fuselage for a few Mach numbers.

metric nature of the monopole, it is easier to evaluate the incident pressure by using a cylindrical axis that goes through the monopole. The incident freefield pressure on this coordinate system is in the form of out-going axisymmetric waves with angular mode $n=0$ and is given by

$$p_{i\omega}(1) = \int_{-\infty}^{\infty} D_0 H_0^{(1)}(\zeta y) e^{ik_x x}\, dk_x \qquad (24)$$

where

$$D_0 = \frac{1}{8\pi}(\omega - Mk_x) e^{-ik_x x_0} q_\omega$$

and for a point on the fuselage surface

$$y = \left[r_0^2 - 2r_0 \cos(\theta - \theta_0) + 1\right]^{1/2}$$

in Eq. (24). Numerical examples showed good agreement between Eq. (11) and Eq. (24) for a monopole.

Results

A computer program was used to perform the calculations as described in the Analysis for the case of a monopole source outside the boundary layer. Examples were used to illustrate various aspects of the fuselage and its boundary-layer effects on SPL. For the convenience of comparisons, a typical example is used as a reference case. Parameters were varied one at a time to illustrate the differences.

For evaluating the effects on fuselage surface SPL and on enroute noise, a typical example is chosen to have the following parameters:

freestream Mach number $M=0.7$
fuselage radius $R_f=8$ ft
boundary layer thickness $L=1$ ft
Pohlhausen boundary-layer velocity profile;

$$U(r) = M\left[2\left(\frac{r-1}{r_b-1}\right) - 2\left(\frac{r-1}{r_b-1}\right)^3 + \left(\frac{r-1}{r_b-1}\right)^4\right]$$

freestream temperature $T_0=400$ R
isothermal boundary layer ($c_f/c_0=1$)
monopole location $r_0=R_0/R_f=1.5$, $\theta_0=0$, $x_0=0$
source frequency $f=250$ Hz ($\lambda_0/R_f=0.49$)

For community noise, $M=0.3$ and $T_0=520$ R were used.

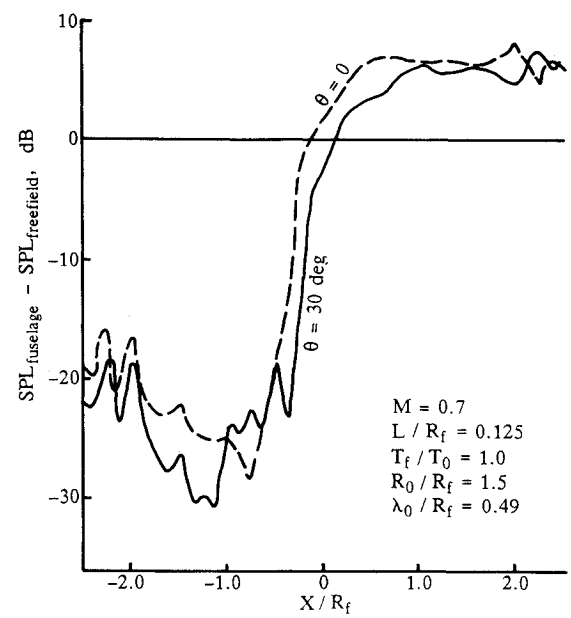

Fig. 5 Variation of effects along the fuselage at two different azimuthal angles.

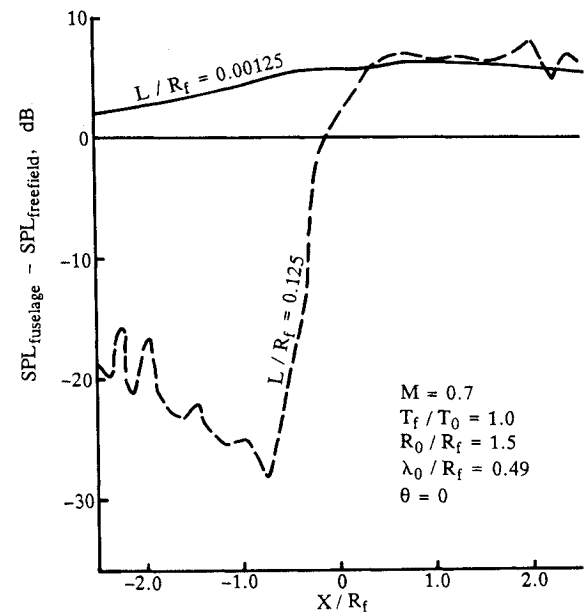

Fig. 6 Boundary-layer thickness effects.

SPL on Fuselage Surface

The dimensionless amplitudes of the acoustic pressure on the fuselage surface and of the freefield around a cross section at the source location station are compared in Fig. 2. On the source side, directly underneath the source, the surface SPL is higher than that of the freefield; however, the fuselage and its boundary layer cause a "shadow" toward the far (opposite) side of the fuselage. Notice that the amplitude on the surface reaches a minimum at about $\theta = 100$ deg, and rises slightly in the back "shadow" side.

Longitudinal distributions of the amplitudes of the dimensionless acoustic pressure, Eqs. (10) and (24) with $q_\omega = 1$, are compared in Fig. 3 for the fuselage element directly underneath the source. It appears that the boundary layer shifts the distribution in a downstream direction and, therefore, causes a strong attenuation in the upstream direction and an amplification in the downstream direction. The difference in the peak values is small, i.e., the fuselage surface peak acoustic pressure is only slightly greater than that of the freefield. The surface acoustic pressure would be twice that of the freefield for the case of an infinite flat plate without a boundary layer. Notice, also, that due to the presence of the flow the monopole acoustic field is skewed toward the forward direction. The peak is in front of the source.

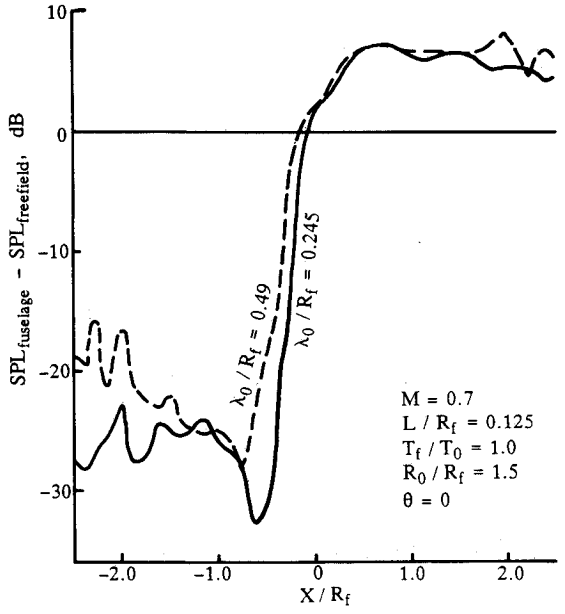

Fig. 7 Effects for two different frequencies.

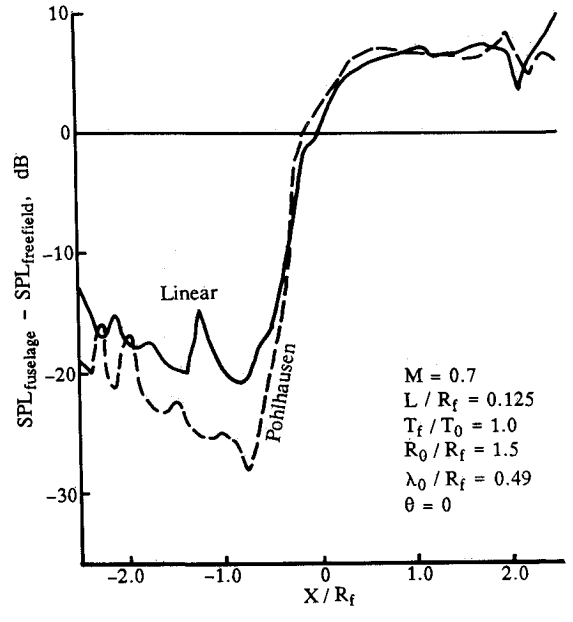

Fig. 8 Boundary-layer velocity profile effects.

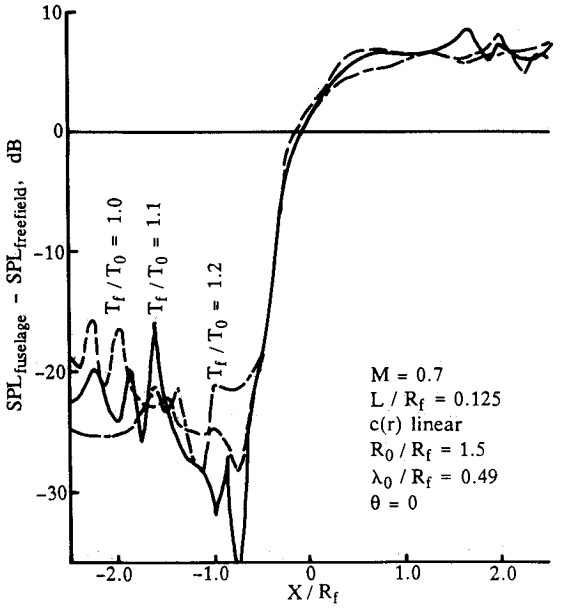

Fig. 9 Boundary-layer temperature effects.

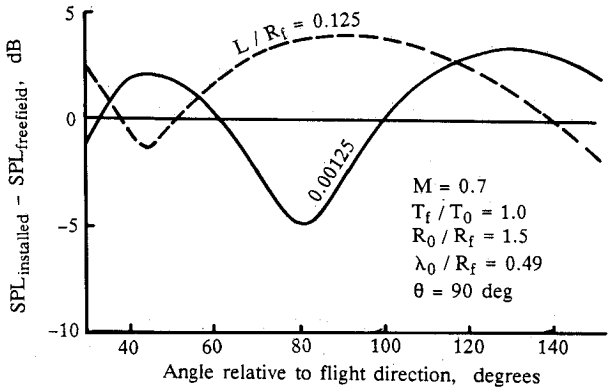

Fig. 10 Boundary-layer thickness effects on enroute noise.

The variation of the effects, Eq. (12), with changes in freestream Mach numbers is shown in Fig. 4. Attenuation in the forward direction increases rapidly with increasing freestream Mach number. In the downstream direction, the SPL increase is aproximately 6 dB above the freefield levels. Strong oscillations of the curves are caused by integration across the eigenvalues of $E = 0$ in Eq. (9), related to the neutral stability of the boundary layer for real k_x. It is found, for all the cases calculated, that $E = 0$ occurs only when ζ in Eq. (5) is imaginary.

Comparison of the effects along the fuselage was made for two azimuthal angles, as shown in Fig. 5. As expected, the offset position at 30 deg has stronger effect, due to the fuselage curvature and the longer propagation distance through the boundary layer, than the zero degree case.

The effects of boundary-layer thickness are compared in Fig. 6. For a boundary layer of negligible thickness, the forward attenuation effects are much weaker than that of a thick one.

As expected, the forward attenuation increases with increasing frequency. This is shown in Fig. 7 for two frequencies at one octave apart. It should be noticed that the wavelength varies with the wave propagation direction and the local Mach number.

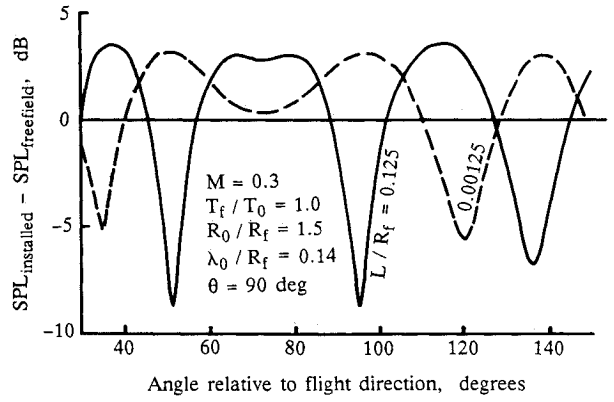

Fig. 11 Effects on community noise, 1000-Hz source frequency.

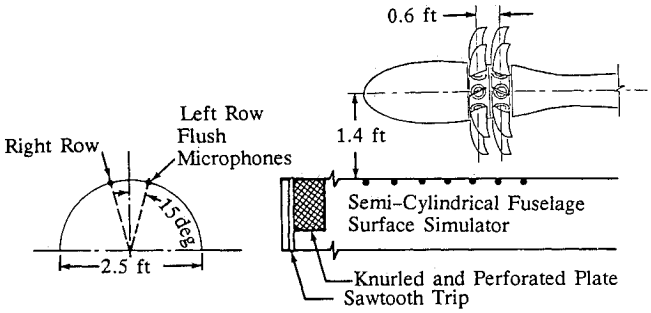

Fig. 12 Schematic test layout in the transonic wind tunnel.

Effects in varying the boundary-layer velocity profile within a reasonable range are not strong, as shown in Fig. 8 by comparing the Pohlhausen and the linear profiles. The linear profile shows more attenuation in the "propagating" region underneath the source. Pohlhausen profile provides more "shielding" in the forward direction.

Variation in temperature across the boundary layer in a range that can occur in actual flight conditions does not show significant effect on noise attenuation. Figure 9 shows the effects for three different fuselage wall to freestream temperature ratios.

Effects on Enroute Noise

The effects in the farfield were calculated by using Eq. (16). For enroute noise, a cruise Mach number of 0.7 was used. To simulate an engine mounted on the side of the fuselage, the observer under the flight path is at $\theta = 90$ deg, as indicated in Fig. 10, which compares the effects of the boundary layer of two different thicknesses: a normal one and a very thin one. The farfield wave normal angles relative to the flight direction are indicated on the horizontal axis. The boundary layer strongly alters the farfield interference pattern caused by the fuselage.

Effects on Airport Community Noise

The effects on community noise level are compared in Fig. 11 for a source frequency of 1000 Hz. A flight Mach number of 0.3 was used for calculation to represent a takeoff case. The "installation" effect can reach 3 to 4 dB. Even at this low Mach number, the boundary-layer thickness effect is still strong enough to shift the directivity pattern.

Comparison with Model Test Data

A counter-rotating propeller model was tested in a transonic wind tunnel. A schematic of the test layout is shown in Fig. 12. The fuselage was simulated by a 2.5-ft diameter semicylindrical plate. A model propeller diameter is approximately 2 ft. Two rows of flush microphones at 15 deg from each side of the centerline, as indicated in the sketch, were used. The left row was facing the leading edges of the oncoming front rotor, which runs in a left-hand screw direction. The right row was facing the oncoming leading edges of the aft rotor, which runs in a right-hand screw direction. Boundary layers of different thicknesses were generated by using a smooth surface, a knurled and perforated plate, and a sawtooth trip. The boundary-layer profiles at a location 45 deg relative to the propeller forward axis from the aft-rotor center are shown in Fig. 13. Estimated values of the boundary-layer thickness were $L = 0.1$ ft for the smooth surface, $L = 0.2$ ft for the knurled and perfo-

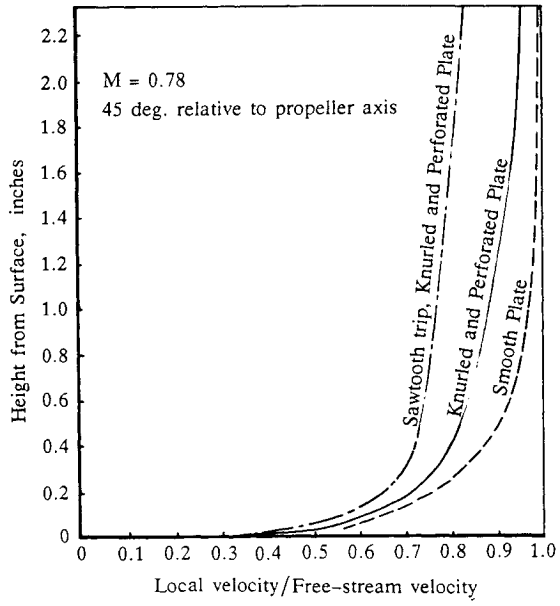

Fig. 13 Boundary-layer profiles on fuselage simulator surface.

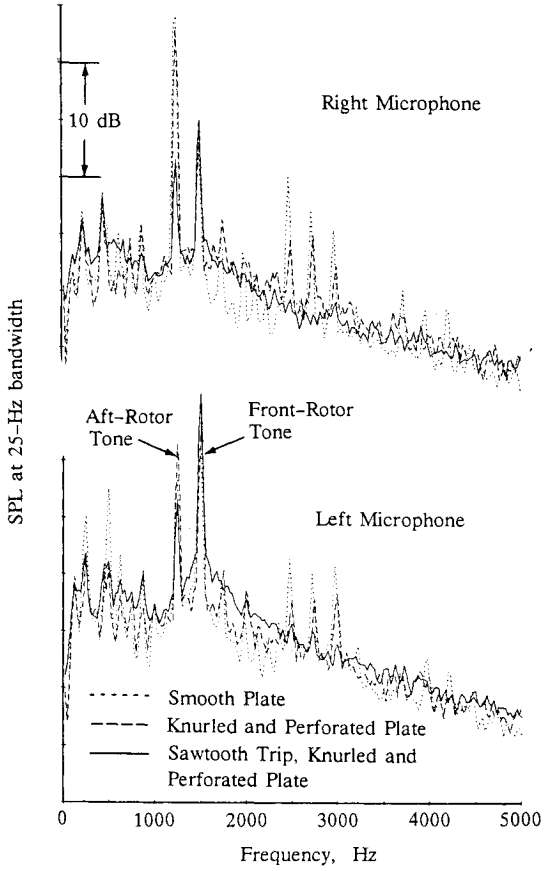

Fig. 14 Counter-rotating model propeller noise on fuselage simulator surface.

rated plate, and $L = 0.4$ ft for the sawtooth trip with the knurled and perforated plate. These values were used in calculating the boundary-layer effects.

Narrow-band spectra from the flush microphones 47 deg relative to the propeller axis from the aft-rotor center are shown in Fig. 14 for the case at Mach number of 0.78. The right microphone, facing the oncoming leading edges of the aft-rotor shows a 10-dB attenuation for the sawtooth trip over the other two configurations. The attenuation is about 5 dB on the left side, as shown in Fig. 14. Calculations for this case by using a monopole source provide 5.4 and 5.8 dB, respectively, for the knurled and the sawtooth configurations over the smooth configuration. There are many factors that can cause the difference between test data and the calculated values. The propeller tone directivity, the distributed nature of the propeller noise source, the presence of the model nacelle, and the turbulent boundary in real test are different from the idealized analytical model.

Boundary layer of all the three configurations in the test were able to shield the propeller tones for all the angles 36 deg or less from the forward; i.e., the tones were lower than the broadband levels. This trend is consistent with the calculation. Essentially, no difference in tone levels in the aft-arc for different boundary-layer thickness was observed from the test data. This trend also agrees with the calculation.

Conclusion

The present analysis, based on an idealized model, is used to illustrate the scattering and refraction effects of a fuselage and its boundary layer. The turbulence in a real fuselage boundary layer may have some effects on sound of wavelength comparable or smaller than the size of the turbulent eddies. However, this occurs only in the high frequencies or high harmonics of the propeller tones.

Variations in fuselage diameter and boundary-layer thickness along the flow direction are assumed to be slow and can be treated as parametric variations, since this analytical model does not allow axial variations in mean quantities.

The formal solutions have been obtained for a given incident, free acoustical field expressed on the fuselage center coordinates. An acoustic field expressed in another coordinate system has to be re-expressed in this coordinate axis in order to use the solutions. This usually involves expansions in a series of Bessel functions and increases the computation time. From the monopole source calculations, the trends are in agreement with the propeller test data.

Appendix: Coefficients of Frobenius Series

At a point $r = r_c$, where $\omega - U(r_c)k_x = 0$, let

$$U(r) = U(r_c) + U'(r_c)z + \tfrac{1}{2}U''(r_c)z^2 + \cdots$$

$$c(r) = c(r_c) + c'(r_c)z + \tfrac{1}{2}c''(r_c)z^2 + \cdots$$

where

$$z = r - r_c \quad \text{for} \quad r > r_c$$

$$z = (r_c - r)e^{-i\pi} \quad \text{for} \quad r < r_c$$

The Frobenius series is expressed to the third order in z as

$$S = a[g_0 + g_2 z^2 + z^3 \ell n(z)] + bz^3 + \cdots$$

where, for a matching point $r = r_m < r_c$ but very close to r_c,

$$a = F(r_m)/g_0$$

$$b = \frac{F'(r_m)}{3(r_c - r_m)^2} + \frac{2g_2 F(r_m)}{3(r_c - r_m)g_0} - [1 + 3\ell n(r_c - r_m)]\frac{F(r_m)}{3g_0}$$

$$g_0 = \frac{5}{(p_2 + q_1)n_1 + n_2}$$

$$g_2 = n_1 g_0/2$$

$$p_2 = \frac{U''(r_c)}{2U'(r_c)}$$

$$q_1 = \frac{1}{r_c} + \frac{2c'(r_c)}{c(r_c)} - \frac{2U''(r_c)}{U'(r_c)}$$

$$n_1 = -k_x^2 - \frac{n^2}{r_c^2}$$

$$n_2 = \frac{2n^2}{r_c^3} + \frac{U''(r_c)k_x^2}{2U'(r_c)}$$

References

[1]Hanson, D. B. and Magliozzi, B., "Propagation of Propeller Tone Noise Through a Fuselage Boundary Layer," *Journal of Aircraft,* Vol. 22, Jan. 1985, pp. 63–70.

[2]McAninch, G. L. and Rawls Jr., J. W., "Effects of Boundary Layer Refraction and Fuselage Scattering on Fuselage Surface Noise from Advanced Turboprop Propellers," AIAA Paper 84-0249, AIAA 22nd Aerospace Science Meeting, Jan. 1984.

[3]McAninch, G. L., "Effects of Velocity Profile on Boundary Layer Shielding," AIAA Paper 87-2678, AIAA 11th Aeroacoustics Conf., Oct. 1987.

[4]Goldstein, M. E., *Aeroacoustics,* McGraw-Hill, NY, 1976.

[5]Carrier, G. F., Krook, M., and Pearson, C. E., *Functions of a Complex Variable,* McGraw-Hill, NY, 1966.